Detecting codimension-two objects in an image with Ginzburg-Landau models

Gilles AUBERT [1] & Jean-François AUJOL [1,2] & Laure BLANC-FÉRAUD [2]

[1] Laboratoire J.A.Dieudonné, UMR CNRS 6621, Université de Nice Sophia-Antipolis
Parc Valrose, 06108 Nice Cedex 2 , France
email: {gaubert,aujol}@math.unice.fr

[2] ARIANA, projet commun CNRS/INRIA/UNSA, INRIA Sophia Antipolis
2004, route des Lucioles, BP93, 06902, Sophia Antipolis Cedex, France
email: {Jean-Francois.Aujol,Laure.Blanc_Feraud}@sophia.inria.fr

Abstract

In this paper, we propose a new mathematical model for detecting in an image singularities of codimension greater than or equal to two. This means we want to detect points in a 2-D image or points and curves in a 3-D image. We drew one's inspiration from Ginzburg-Landau (G-L) models which have proved their efficiency for modeling many phenomena in physics. We introduce the model, state its mathematical properties and give some experimental results demonstrating its capability.

Key-words: Ginzburg-Landau model, points detection, segmentation, PDE, biological images, SAR images.

1. Introduction

The goal of this paper is to propose a new mathematical model for detecting in an image singularities of codimension greater than or equal to two. This means we want to detect points in a 2-D image or points and curves in a 3-D image. To the best of our knowledge there exist in the literature few works tackling this problem. Most of existing models are devoted to the detection of singularities of codimension-one, e.g. curves in $\mathbb{R}^2$ or surfaces in $\mathbb{R}^3$. Recently Lorigo et al [16] have developed a codimension-two geodesic active contour scheme for the segmentation of thin structures. Their algorithm is based on work in differential geometry [3] concerning the evolution of arbitrary dimensional manifolds in arbitrary dimensional space. See also [19] for a diffusion-generated motion scheme for codimension-curves. Lorigo et al have applied their algorithm for automatically segmenting blood vessels in volumetric resonance angiography images.

Here our approach is quite different.We drew one's inspiration from Ginzburg-Landau (G-L) models which have proved their efficiency for modeling many phenomena in physics and in particular in the theory of superconductors. Though our final objective is to treat 3D-images we focus in this paper on 2D-images. We introduce the model, state its mathematical properties and give some experimental results demonstrating its capability. Actually there exists a general theory of G-L models involving functions u from $\mathbb{R}^{n+k}$ into $\mathbb{R}^k$ for the study of singularities of codimension-k in an ambient space of dimension $n+k$ (see [2]).

Here we will mainly examine the case $k=2$ and $n=0$. However we will also show some experiments in the case $k=1$ and $n=1$. In the latter situation we will see that our algorithm is able to detect curves which are not necessarily closed and that we can also capture certain quadruple junctions. Moreover our approach is quite general since we could treat noisy images. The plan of the paper is organized as follows.

In section 2 we introduce the G-L model and give its main physical and mathematical properties. Then in section 3 we show how such a model can be adapted to the detection of points in 2-D images. In section 4 we display some numerical results demonstrating that our algorithm also applies for the detection of curves in 2-D images and in particular its capability to process the detection of non-closed curves.

2. The Ginzburg-Landau model

In this section we introduce the Ginzburg-Landau model. We first present the origin of the model, then we give its main mathematical properties and finally we show how this model can be used for detecting in an image singularities of codimension-two. For the in-

troduction of the model we follow [20].

The Ginzburg-Landau was designed in the fifties by Ginzburg and Landau [13] to modelize phenomenological patterns in superconductor material near their critical temperature. Semiconductors have the particularity that when they are cooled down below a critical temperature they become " superconducting " which means that there can be permanent currents without dissipation. A common simplification is to restrict to the two-dimensional case by considering a section $\Omega \subset \mathbb{R}^2$ of an infinite cylindrical domain of $\mathbb{R}^3$. The behaviour of the material submitted to an external field h_{ex} is modeled through the minimization of an energy which is, after renormalization:

$$J(u,A) = \frac{1}{2}\int_\Omega (\,|\nabla u - i\,Au|^2 + \frac{1}{2\varepsilon^2}(1-|u|^2)^2)\,dx + \int_{\mathbb{R}^2} |h-h_{ex}|^2)\,dx \qquad (2.1)$$

where A is the vector potential, and $h = curl\, A$ the induced magnetic field. The parameter ε, called the coherence length, is a small dimensionless constant depending only of the material and of the temperature. u is a complex-valued function which indicates the local state of the material: if $|\,u(x)\,| \simeq 1$ the material is in a superconducting phase while if $|\,u(x)\,| \simeq 0$ it is in its normal phase (with no superconducting property). A rigorous mathematical study of the behavior of the minimizers of the G-L functional shows that there exists a phase-transition between these two previous states. This transition depends on two critical values $h_1 = O(\,|\log\varepsilon|\,)$ and $h_2 = O(\,\frac{1}{\varepsilon^2}\,)$. If $h_{ex} < h_1$ the material is superconducting: $|\,u(x)\,| \simeq 1$. If $h_{ex} = h_1$ there is a phase transition where coexist normal and superconducting phases. The normal phase is localized in small regions of characteristic size ε called " vortices " surrounded by superconducting regions. At the center of the vortex $|\,u\,| \simeq 0$. When $h_{ex} = h_2$ the superconductivity disappears $|\,u\,| \simeq 0$ and $h = h_{ex}$.

At this stage the reader could think we are far from image analysis problems. In fact G-L functionals have been used in many areas of physic or chemistry. Moreover G-L models have already been used for image inpainting tasks [15, 14]. Let us note incidentally that there exist other works in image processing using complex-values functions (see for example [12]). May be what it is important to keep in mind is that G-L models are able to capture singularities, e.g. vortices or singularities of codimension 2 in $\mathbb{R}^2$ or $\mathbb{R}^3$. To better understand such a phenomenon it would be timely to state some mathematical results. There exists an important literature concerning G-L models. It is not the place here to review all these results. We will only give those which are the most linked to our purpose. Most of them rely on the simplified energy:

$$E_\varepsilon(u) = \frac{1}{2}\int_\Omega (\,|\nabla u|^2 + \frac{1}{2\varepsilon^2}(1-|u|^2)^2)\,dx \qquad (2.2)$$

or on the associated flow governed by the evolution equation:

$$\frac{\partial u}{\partial t} = \Delta u + \frac{1}{\varepsilon^2} u\,(\,1-|u|^2) \qquad (2.3)$$

In order to avoid trivial solution and to get singularities we need to add some (singular) data. With the functional (2.2) Dirichlet data $u(x) = u_0(x)$ on the boundary $\partial\Omega$ are often associated, but Neumann conditions can also be used. Instead of Dirichlet conditions we can incorporate in (2.2), as we will do later, a data term of the type $\int_\Omega |u-u_0|^2\,dx$. For (2.3) we need to define an initial condition at $t=0$: $u(x,0) = u_0(x)$ as well as boundary conditions.

We now state some typical mathematical results for (2.2). We give a result due to Bethuel-Brezis-Helein [8]. It concerns functional (2.2) with a Dirichlet condition. Though Dirichlet condition is not very realistic in physical situations, this case reflects well the general behavior of minimizers of the G-L functional. We denote by $d = \deg(u_0, \partial\Omega)$ the Brouwer degree) (see Appendix A for the definition of the Brouwer degree) of u_0 around $\partial\Omega$.

We will identify the Sobolev space $H^1(\Omega\,;\mathbb{C})$ to $H^1(\Omega\,;\mathbb{R}^2) = \{u : \Omega \to \mathbb{R}^2;\ u \in L^2(\Omega)^2$ and $\nabla u \in L^2(\Omega)^4\}$ where ∇u stands for the distributional Jacobian of u [1]. We will denote by $H^1_{u_0}(\Omega\,;\mathbb{R}^2))$ the set of functions u in $H^1(\Omega\,;\mathbb{C})$ such that $u = u_0$ on $\partial\Omega$.

We first state the result and then we will try to give an intuitive explanation of it.

Theorem 2.1. *[8]*

Assume that $\Omega \subset \mathbb{R}^2$ is convex, $|\,u_0| = 1$ and $d = \deg(u_0, \partial\Omega) > 0$, then

1. *Functional (2.2) has a minimizer u_ε in $H^1_{u_0}(\Omega\,;\mathbb{R}^2))$. Moreover u_ε has exactly d zeroes in Ω and each one is of degree 1.*

2. *There is a subsequence $\varepsilon_n \to 0$ and exactly d points $a_1, a_2, ..., a_d$ in Ω and a smooth function u_* from $\Omega\backslash\{a_1, a_2, ..., a_d\}$ with $|u_*| = 1$, $-\Delta u_* = u_*\,|\nabla u_*|^2$, and $u = u_0$ on $\partial\Omega$ such that*

$$u_{\varepsilon_n} \to u_* \text{ in } C^k_{loc}(\Omega\backslash\{a_1, a_2, ..., a_d\}),\ \ \forall k$$

In fact in [8] there are many other results concerning for example bounds for the energy or the localization of singularities.

Let us now comment the above result. Roughly speaking the theorem tells us that we are able to construct a sequence u_{ε_n} such that for ε_n small enough $|u_\varepsilon| \approx 1$ almost everywhere and u_{ε_n} has d zeroes which could be understood as singularities. These singularities are the consequence of the assumption $d = \deg(u_0, \partial\Omega) > 0$. Brouwer or topological degree is a mathematical tool which is used to prove the existence of solutions for equations in $\mathbb{R}^n$ or in Banach spaces. By using the notion of degree we can prove the following result which is closely related to our purpose : let us consider a bounded and simply connected domain Ω in $\mathbb{R}^2$ and a smooth mapping $g : \partial\Omega \to S^1$, where $S^1 = \left\{x \in \mathbb{R}^2;\ |x| = 1\right\}$. If $\deg(g, \partial\Omega, 0) \neq 0$, then there does not exist $u \in H^1(\Omega;\ \mathbb{C})$ such that $u_{/\partial\Omega} = g$ which implies that $H^1_g(\Omega;\ \mathbb{C}) = \emptyset$. When $\Omega = \{x;\ |x| < 1\}$ and $g(x) = x$ this result means that there is no retraction of the disc onto its boundary. Geometrically this also means there is a topological obstruction and this may be the cause in Theorem 2.1 of the creation of singular points.

Of course in image analysis we generally do not use Dirichlet conditions and the previous theorem does not apply directly but it tells us that singularities in data can be detected by such a model.

3. Detection of singularities of codimension-2 in 2-D images

Let us now go back to the problem of detecting singularities of codimension-two in a 2-D image. First, we have from an initial 2-D image $f(x)$ to construct a complex-value image u_0 (we only consider gray-level image). There are many ways for doing it. We choose the one's proposed by [15]. We first rescale the intensity image $f(x)$ to the interval $[-1, 1]$, then $f(x)$ is identified with the real part of a complex valued function u_0: $\Omega \to \mathbb{C}$ by defining $Im(u_0) = \sqrt{1 - f(x)^2}$, so that $|u_0| = 1$. For detecting singularities of codimension-two (points) we propose to search for minimizers $u_\varepsilon \in H^1(\Omega;\ \mathbb{C})$ of the following G-L functional :

$$\begin{aligned} F_\epsilon(u) &= \mu \int_\Omega a(x) |\nabla u|^2 + \frac{1}{\epsilon^2} \int_\Omega \left(1 - |u|^2\right)^2 \\ &\quad + \frac{\lambda}{2} \int_\Omega |u - u_0|^2 \end{aligned} \tag{3.1}$$

where $a(x)$ is a diffusion coefficient. If we denote by u (for the sake of clarity, we omit the ϵ dependence) a minimizer of $E_\varepsilon(u)$ then it satisfies the Euler-Lagrange system :

$$-\mu \mathrm{div}\left(a(x)\nabla u\right) - \frac{1}{\epsilon^2} u\left(1 - |u|^2\right) + \lambda\left(u - u_0\right) = 0 \ \text{ in } \Omega \tag{3.2}$$

and $\frac{\partial u}{\partial N} = 0$ on $\partial\Omega$ (where N is the outward unit normal to $\partial\Omega$).

In the original Ginzburg-Landau functional, there is no diffusion coefficient. The main reason for which we introduce $a(x)$ comes from the fact that we do not impose Dirichlet condition on the boundary $\partial\Omega$ of Ω, and then the natural boundary condition associated to the minimization of F_ϵ is a Neumann boundary condition: $\frac{\partial u}{\partial N} = 0$ on $\partial\Omega$. In this case, as pointed out by [11], it may happens that vortices of initial data can eventually disappear from the domain (for example a vortex can merge with other vortices). Hence to stabilize each vortex we need to create an energy barrier around the vortex by choosing an appropriate diffusion coefficient $a(x)$. Here as vortices are essentially created by discontinuity points, we choose $a(x)$ as follows:

$$a(x) = W(\Delta f) \tag{3.3}$$

where f is the initial gray level image and W is a non-increasing function with $W(0) = 1$ and $W(+\infty) = 0$. Typically, we choose

$$W(t) = \frac{1}{1 + (t/\alpha)^2} \tag{3.4}$$

where α is a parameter modelling the size of the discontinuity. Moreover, since f may not be twice differentiable (in fact f is not continuous at points we want to detect), we first smooth it by convolution with a Gaussian kernel before computing W.

3.1 Evolution equation

As it is often used, to solve (3.2), we embed it into a dynamical scheme :

$$\frac{\partial u}{\partial t} = \mu \mathrm{div}\left(a(x)\nabla u\right) + \frac{1}{\epsilon^2} u\left(1 - |u|^2\right) - \lambda\left(u - u_0\right) \tag{3.5}$$

with Neumann boundary conditions and initial condition $u(t = 0, x) = u_0(x)$.

We write $u = (u_1, u_2)$, so that we can rewrite (3.5) as:

$$\left\{\begin{array}{ll} \frac{\partial u_1}{\partial t} = & \mu \mathrm{div}\left(a(x)\nabla u_1\right) + \frac{1}{\epsilon^2} u_1\left(1 - \left(u_1^2 + u_2^2\right)\right) \\ & -\lambda\left(u_1 - (u_0)_1\right) \\ \frac{\partial u_2}{\partial t} = & \mu \mathrm{div}\left(a(x)\nabla u_2\right) + \frac{1}{\epsilon^2} u_2\left(1 - \left(u_1^2 + u_2^2\right)\right) \\ & -\lambda\left(u_2 - (u_0)_2\right) \end{array}\right. \tag{3.6}$$

$(u_0)_1$ is the original image, after it has been rescaled between -1 and 1. We take $(u_0)_2 = \sqrt{1 - (u_0)_1^2}$ (so that $(u_0)_1^2 + (u_0)_2^2 = 1$).

3.2 Discretization of the model

The image is a two dimension vector of size $N \times N$. We denote by X the Euclidean space $\mathbb{R}^{N \times N}$ and $Y = X \times X$. The space X will be endowed with the scalar product $(f, g)_X = \sum_{1 \le i,j \le N} f_{i,j} g_{i,j}$ and the norm $\|f\|_X = \sqrt{(f, f)_X}$. We introduce a discrete version

of the gradient operator. If $f \in X$, the gradient ∇f is a vector in Y given by: $(\nabla f)_{i,j} = ((\nabla f)^1_{i,j}, (\nabla f)^2_{i,j})$

with $(\nabla f)^1_{i,j} = \begin{cases} f_{i+1,j} - f_{i,j} & \text{if } i < N \\ 0 & \text{if } i = N \end{cases}$

and $(\nabla f)^2_{i,j} = \begin{cases} f_{i,j+1} - f_{i,j} & \text{if } j < N \\ 0 & \text{if } j = N \end{cases}$

We also introduce a discrete version of the divergence operator. We define it by analogy with the continuous setting by $\text{div} = -\nabla^*$ where ∇^* is the adjoint of ∇: that is, for every $p \in Y$ and $f \in X$, $(-\text{div}\, p, f)_X = (p, \nabla f)_Y$. It is easy to check that:

$$\begin{aligned} (\text{div}\,(p))_{i,j} &= \begin{cases} p^1_{i,j} - p^1_{i-1,j} & \text{if } 1 < i < N \\ p^1_{i,j} & \text{if i=1} \\ -p^1_{i-1,j} & \text{if i=N} \end{cases} \\ &+ \begin{cases} p^2_{i,j} - p^2_{i,j-1} & \text{if } 1 < j < N \\ p^2_{i,j} & \text{if j=1} \\ -p^2_{i,j-1} & \text{if j=N} \end{cases} \end{aligned} \tag{3.7}$$

Finally, we define a discrete version of the Laplacian operator by setting $\Delta f = \text{div}\,(\nabla f)$ if $f \in X$.

Time discretization: We use an explicit Euler scheme with respect to the time variable t, that is we approximate $\frac{\partial u}{\partial t}$ by $\frac{u^{n+1}_{i,j} - u^n_{i,j}}{\delta t}$ (where n stands for the iteration time).

To solve (3.5), we use an explicit scheme:

$$\begin{aligned} u^{n+1}_{i,j} &= u^n_{i,j} + \delta t \left(\mu(\text{div}\, \left(a_{i,j} u^n_{i,j}\right) \right. \\ &\left. + \frac{1}{\epsilon^2} u^n_{i,j} \left(1 - \left|u^n_{i,j}\right|^2\right) - \lambda \left(u^n_{i,j} - {u^0}_{i,j}\right) \right) \end{aligned} \tag{3.8}$$

with $u^0_{i,j} = (u_0)_{i,j}\ \forall (i,j)$.

We thus get the following system (we omit subindices i, j refering to the pixel location):

$$\begin{cases} u_1^{n+1} = & u_1^n + \delta t \left(\mu(\text{div}\, \left(a\, u_1^n\right)\right. \\ & \left. + \frac{1}{\epsilon^2} u_1^n \left(1 - \left((u_1^n)^2 + (u_2^n)^2\right)\right)\right. \\ & \left. - \lambda \left(u_1^n - (u_0)_1\right)\right) \\ u_2^{n+1} = & u_2^n + \delta t \left(\mu(\text{div}\, \left(a\, u_2^n\right)\right. \\ & \left. + \frac{1}{\epsilon^2} u_2^n \left(1 - \left(\left(u_1^{n+1}\right)^2 + (u_2^n)^2\right)\right)\right. \\ & \left. - \lambda \left(u_2 - (u_0)_2\right)\right) \end{cases} \tag{3.9}$$

3.3 Numerical results

3.3.1 Parameters

We need to fix several parameters before running our algorithm. Fortunately, they have an intuitive explanation which make them easy to fix. We first need to fix the parameters λ, μ and ϵ used in (3.6).

1. ϵ is to be small. We use values ranging from 0.1 to 1.0 (we have mainly used $\epsilon = 0.1$ and $\epsilon = 0.5$). It controls the critical size of the points our algorithm detect, i.e. the resolution of the segmented image. The smaller it is, the finer the resolution is. Nevertheless, one must not set it too small, because the spatial discretization of the image is fixed. Moreover, the smaller ϵ is, the smaller the time discretisation step δt has to be fixed (otherwise, the numerical algorithm does not converge).

2. λ is the fidelity parameter to the initial data. Since we initialize u to u_0, we do not need to use a large value. In our numerical experiments, we have almost always used $\lambda = 0.1$.

3. μ is the regularization parameter. We use values ranging from 0.1 to 50.0 (but we have mainly used $\mu = 1$). It mainly depends on how noisy the initial image is. The larger the noise is, the larger μ should be.

We also need to fix the parameter α in (3.4). It represents the critical size of the step of the discontinuity that our algorithm detects. The larger it is, the larger the detected steps are.

And as we had said, before computing Δf in (3.3), we regularize f by convolution with a Gaussian kernel of standard deviation σ. We use values ranging from 3 to 7. The larger the noise is, the larger we set σ (in the case when the original image has not been degraded by some noise, we sometimes do not regularize f).

3.3.2 Commentaries

On Figure 1, we show an example on a synthetic image: our algorithm catch the points very well. On Figure 2, we have added a Gaussian noise (respectively with standard deviation $\sigma = 10$, 30 and 50). And the algorithm still performs well.

On Figure 3, we show what happens on a real image: we catch the dashes of the leopard. Figure 4 is the same example, but with an additive Gaussian noise with standard deviation $\sigma = 20$. On both examples, the shape of the leopard is given by its dashes.

Figure 5 shows an example of a biologic image. Although we use the model (3.1) which is designed to catch points, we nevertheless detect lines as sequence of points.

Finally, Figure 6 shows an application to SAR interferometry [6]. In this case too, the lines are formed by sequences of points. We will come back to this application in the next section.

4. Detection of codimension-1 structures in 2D-images

As we mentionned in the introduction, in this case, we do not work with complex-values function but with scalar-values functions and we search for a minimizer of (3.1) as a function $u_\varepsilon \in H^1(\Omega;\, \mathbb{R})$.

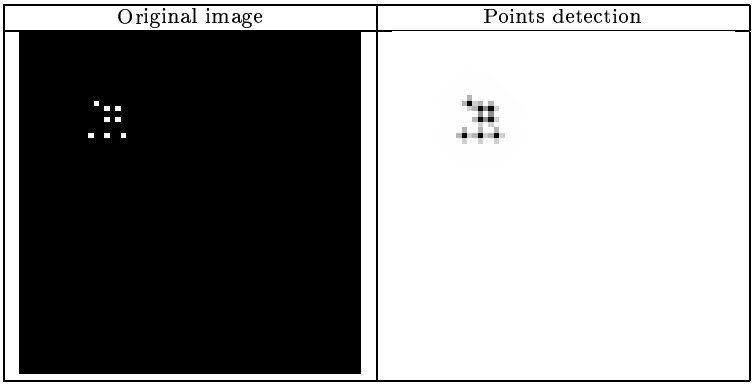

Figure 1: Synthetic image

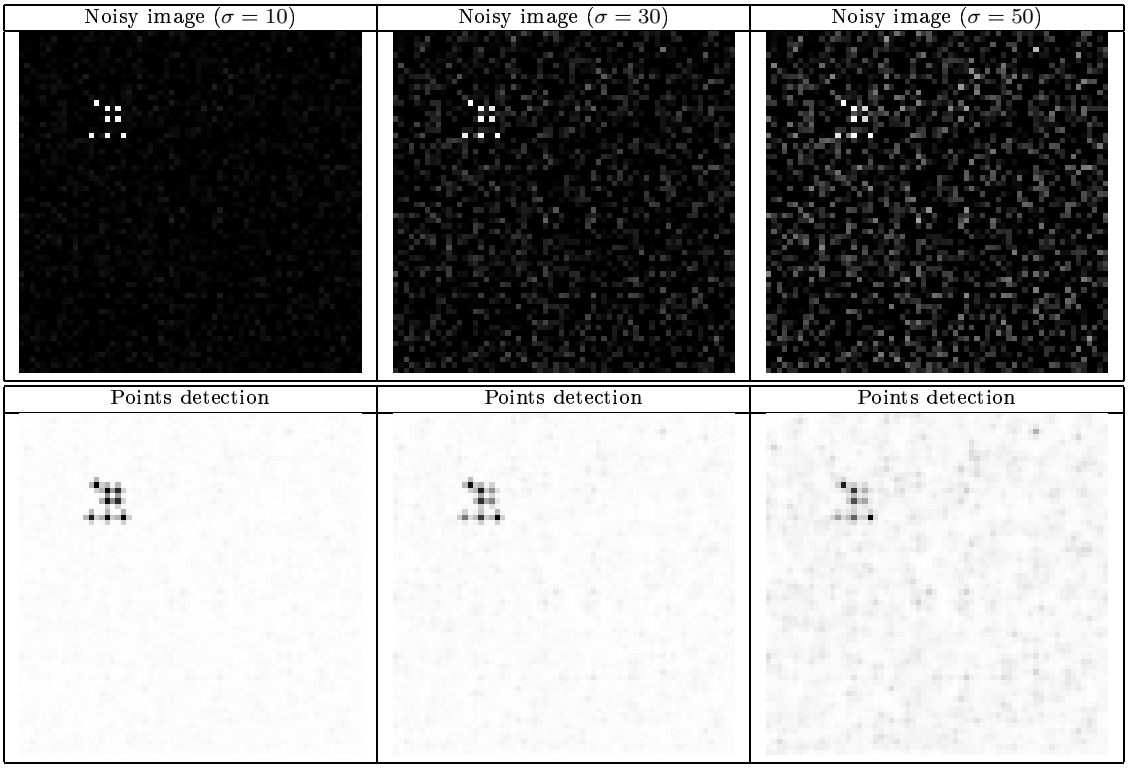

Figure 2: Noisy synthetic images

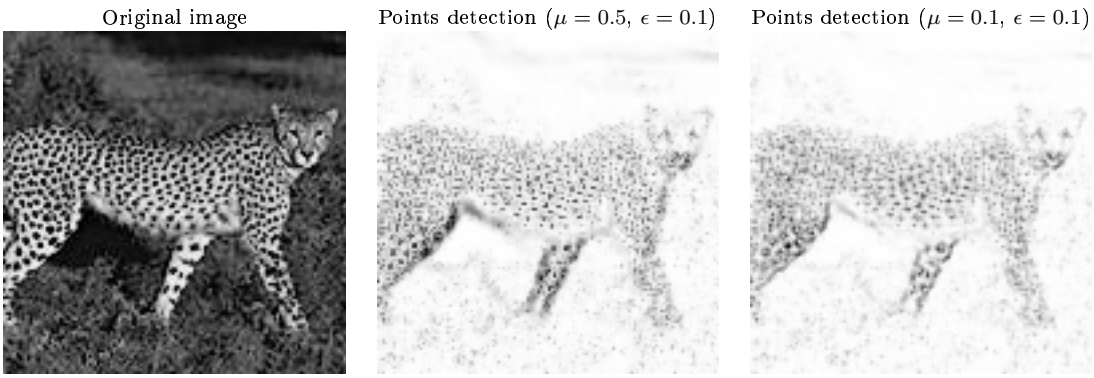

Figure 3: Detecting points

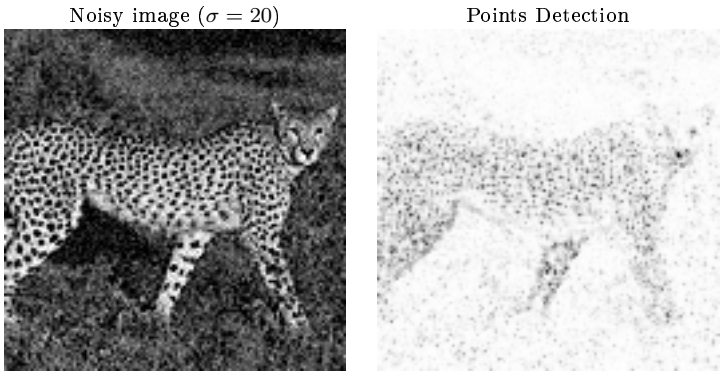

Figure 4: Detecting points in a noisy image ($\sigma = 20$)

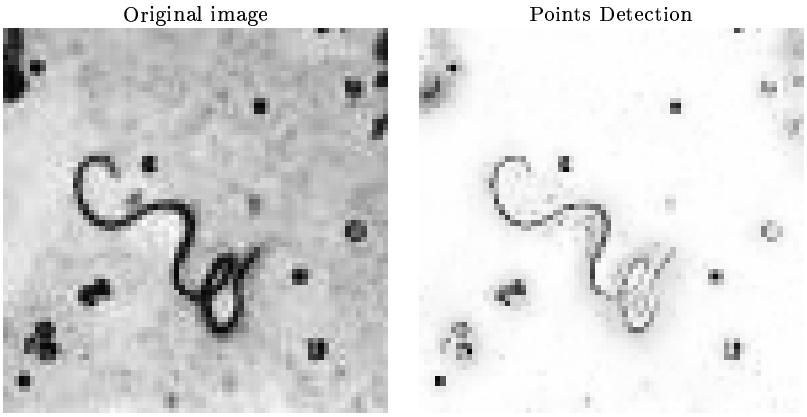

Figure 5: Biological points

Original image

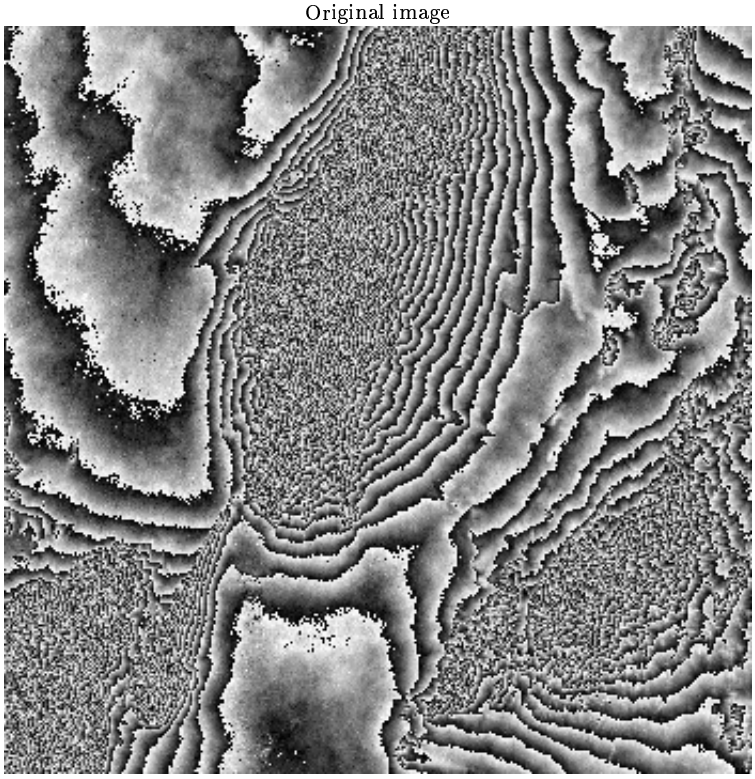

Segmentation

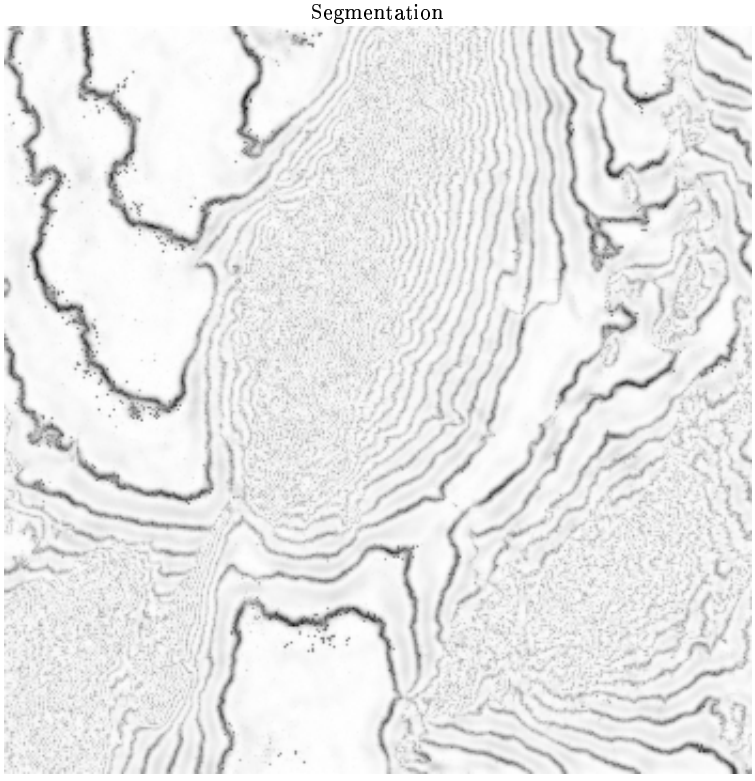

Figure 6: SAR image

In the existing literature, there are many approaches to detect lines in an image. For instance, based on the gradient, there is the classical Canny-Deriche approach [7]. There has also been a lot of approaches using snakes and active contours [9, 7, 10, 4, 21, 18, 17].

We propose here a powerfull algorithm to catch curves in a 2-D image. Comparing with active contours methods, our new algorithm can catch nonclosed curves, and the initilization is completely automatic.

4.1 Evolution equation

As before, we embed PDE (3.2) into a dynamical scheme :

$$\begin{aligned} \frac{\partial u}{\partial t} &= \mu \mathrm{div}\left(a(x)\, u\right) + \frac{1}{\epsilon^2} u\left(1 - |u|^2\right) \\ &\quad -\lambda\left(u - u_0\right) \quad \text{in } \Omega \end{aligned} \tag{4.1}$$

with $\frac{\partial u}{\partial N} = 0$ on $\partial\Omega$. Moreover, we impose $u(t = 0, x) = u_0(x)$. λ and μ are positive weighting parameters. We then discretize (4.1) with finite differences.

In Section 3 we had chosen $a(x) = W(\Delta f)$ (see (3.3)). As the singularities we seek are no longer points but lines, we now choose:

$$a(x) = W(\nabla f) \tag{4.2}$$

where f is the initial gray level image and W is the same function as in Section 3 (see 3.4).

We use the same numerical scheme as in Section 3 (see (3.8), but now the unknown u is a scalar function.

$$\begin{aligned} u_{i,j}^{n+1} &= u_{i,j}^n + \delta t \left(\mu \Delta u_{i,j}^n + \frac{1}{\epsilon^2} u_{i,j}^n \left(1 - \left|u_{i,j}^n\right|^2\right) \right. \\ &\quad \left. -\lambda\left(u_{i,j}^n - {u^0}_{i,j}\right)\right) \end{aligned} \tag{4.3}$$

The initialization u_0 is the original image which has been rescaled between -1 and 1.

4.2 Numerical results

We set the parameters in the same way as in the preceeding section. We have decided to compare our model with the classical Canny-Deriche algorithm. We have used the implemantation in Megawave2 (http://www.cmla.ens-cachan.fr/Cmla/Megawave/).

Figure 7 is an example of segmentation of an image without any noise. One can see that it gives very good edges (comparing with the Canny-Deriche edge detector). The only problem is that our algorithm does not detect the square. We illustrate more precisely this problem on Figures 8 and 9. Figure 8 gives an example of segmentation with a quadruple junction. In this case, the algorithm performs very well. But on can see on Figure 9 that our model cannot handle any quadruple junction. In fact, in many situations, one needs more than two phases. Here, for quadruple junctions we need four phases. In other words, the attracting term in the G-L functional must have four potential wells. Notice that for n-junctions, $n \geq 4$, we only need four potential wells thanks to the four colors theorem. We are currently working on modifying our functional in this direction.

Figure 10 is an example of segmentation of the image of Figure 7 with some Gaussian noise (with standard deviation $\sigma = 20$). The result is still a very good one (because the noise is quite strong).

On Figure 11, we have tested our algorithm on a non-closed curve. We can see that we can detect it, even when there is a strong Gaussian noise (with standard deviation $\sigma = 80$).

Figure 12 is to be compared with Figure 5. One clearly sees that both models do not perform the same way. The model of this section tries to find lines in an image, whereas the model of the previous section aims at finding points. Therefore, in this case, the points are represented by circles, and the lines by their edges (since they have a too large width with respect to the parameter ϵ which has been used).

Figure 13 shows a segmentation result on a biological image. Contrary to Figure 12, the line are represented by a single curve (as in Figure 11). This comes from the width of the lines to be detected and the value of ϵ ($\epsilon = 0.5$ in this case). If we set ϵ smaller, than the lines are considered as objects with non-negligeable width (as in Figure 12 or 7).

We come back to SAR image application [6]. We use our algorithm on the same interferometric image as in Figure 6 (where the original image is displayed). On Figure 14, we see that we get too many lines (in fact, we get twice as many line as we should want). One way to correct this problem is to use the result we get with the point version of the algorithm (Figure 6). Thanks to the previous result, we know which lines we should keep, and which ones we should drop. This give us the result displayed on Figure 15.

5. Conclusion and future prospects

In this paper, we have displayed some experimental results using Ginzburg-Landau functionals for the detection of objects of codimension 2 or 1 in a 2-D image. We got a new model to carry out such tasks. We have also stated some mathematical results about GL models. However these results are not directly applicable to our functional since we do not impose Dirichlet boundary conditions. Therefore it remains to make the complete theoretical study of our model. This will be made in a future work. Our numerical results confirm the ineterest in using such an approach. From a nu-

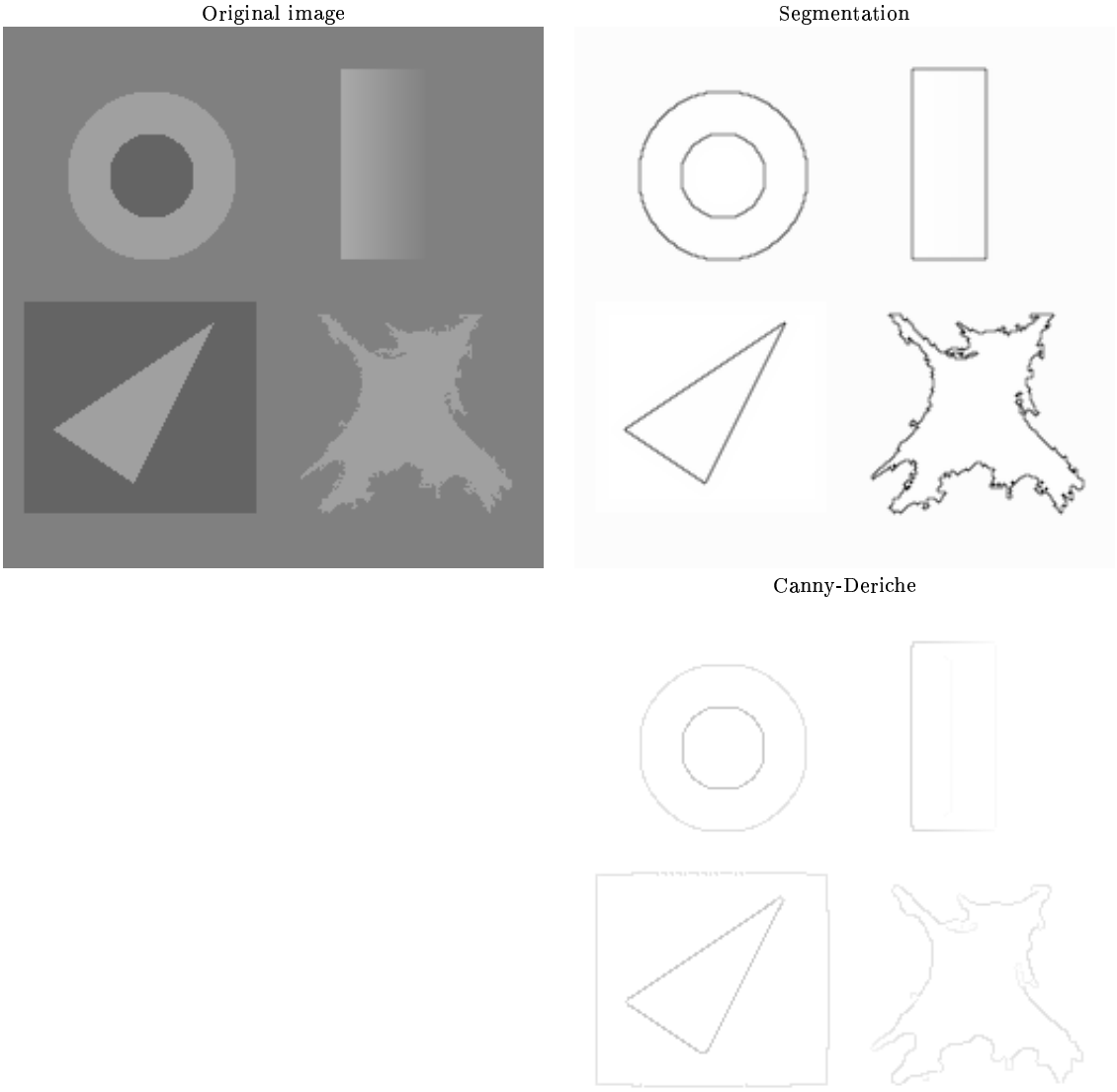

Figure 7: A synthetic image

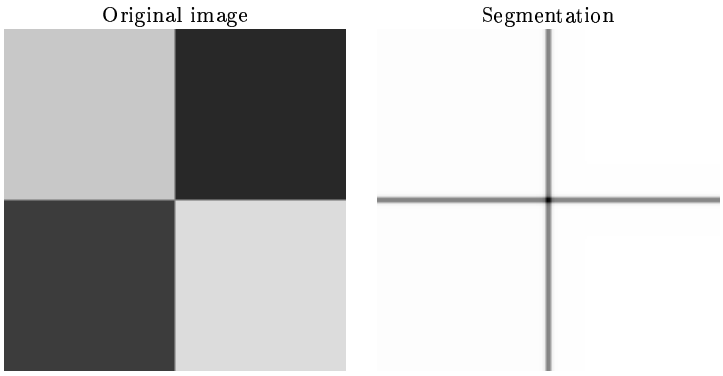

Figure 8: Quadruple junction (good case)

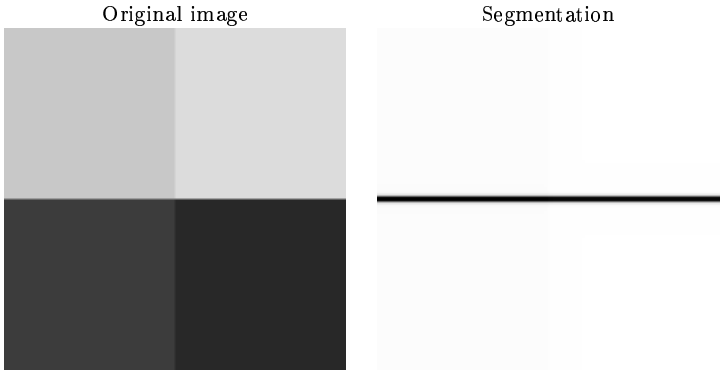

Figure 9: Quadruple junction (wrong case)

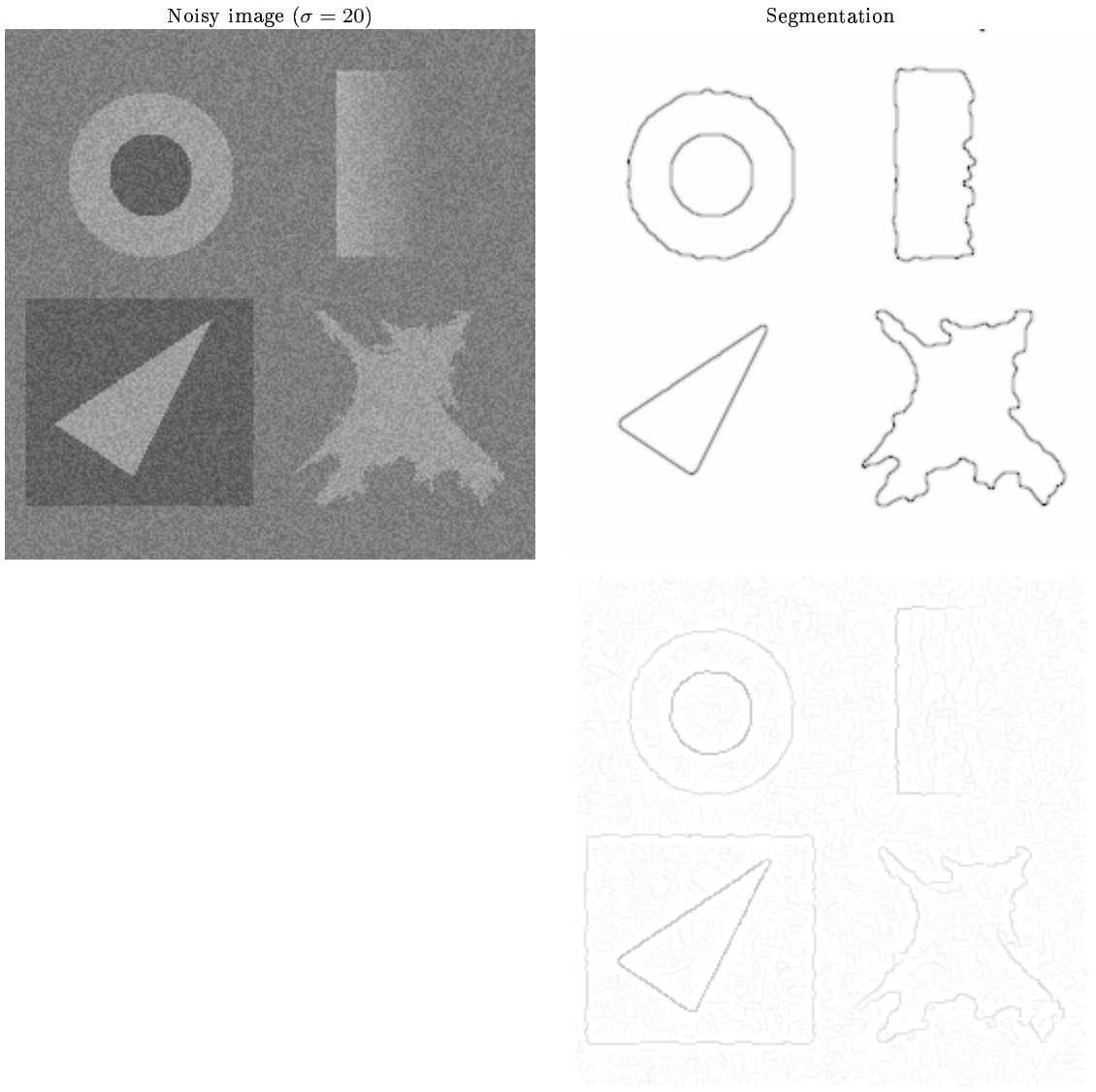

Figure 10: A noisy image

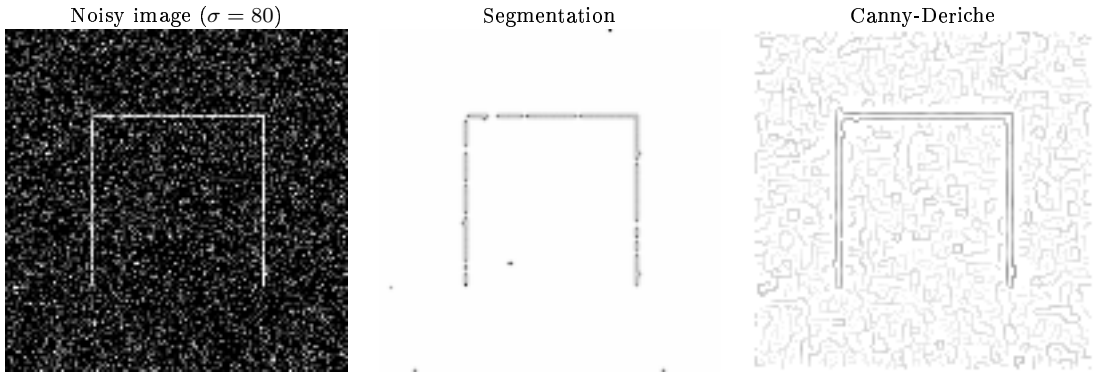

Figure 11: A non-closed curve

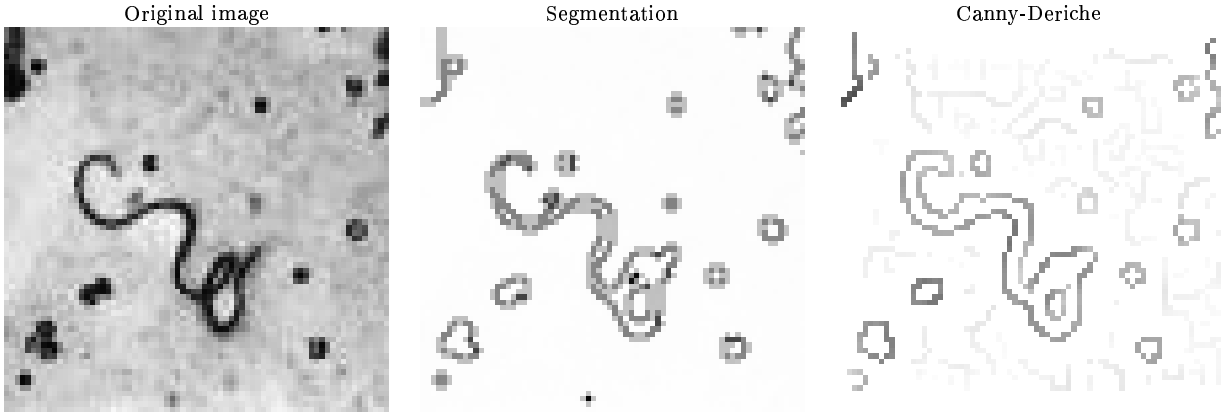

Figure 12: Biological lines

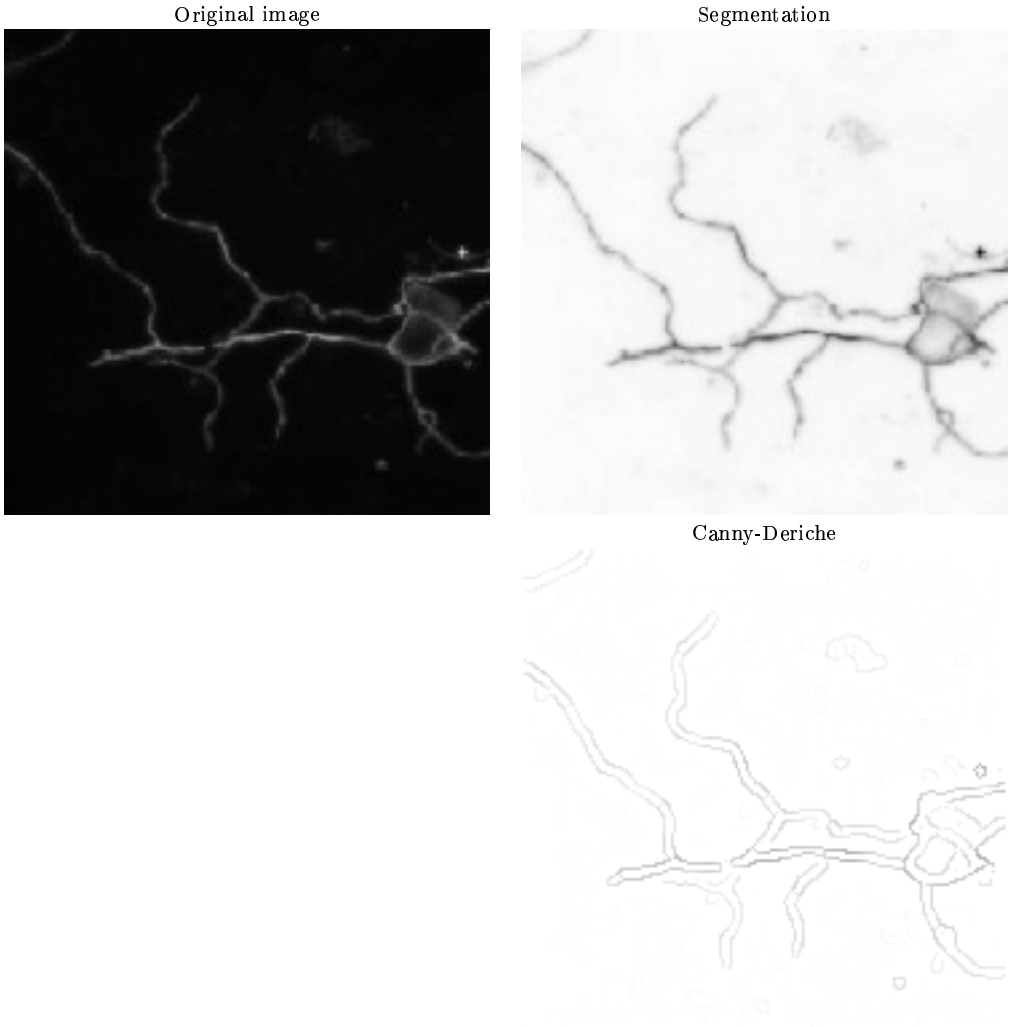

Figure 13: Biological image

Segmentation (Canny-Deriche)

Segmentation

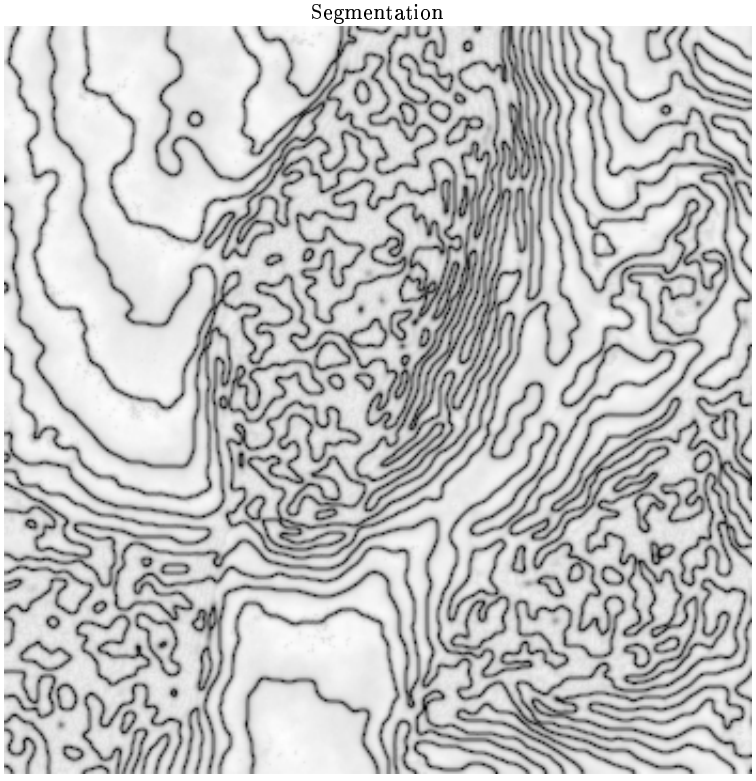

Figure 14: Segmentation of the SAR image

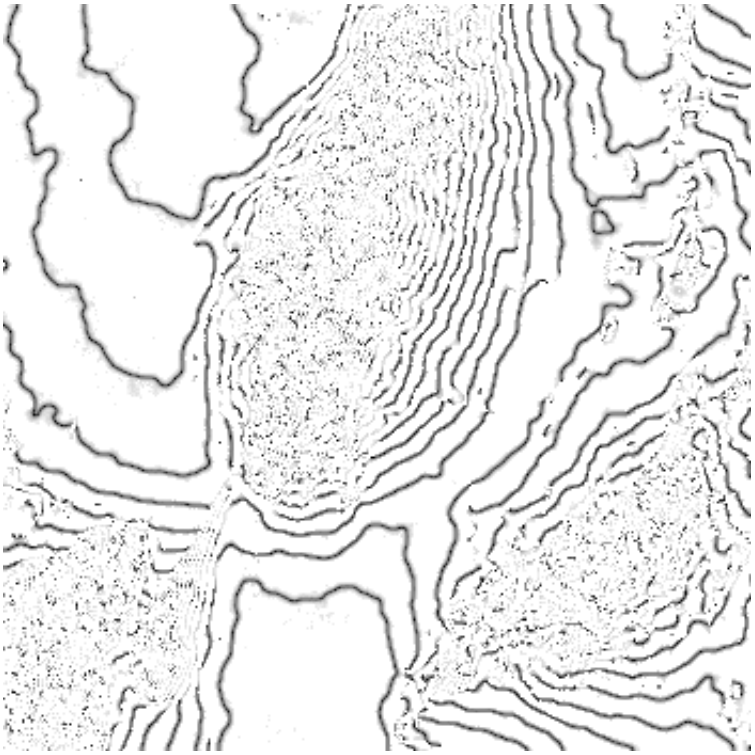

Figure 15: SAR image segmentation using both models

merical point of view, we also have to go further into the tuning of the parameter ϵ. It is closely related to the mesh-size h. We conjecture that a relation of the type $h = O(\epsilon)$ must hold for ensuring the convergence of the discrete functional to the continuous one's. That is why we choose ϵ close to 1 in our experiments since classically in image processing $h = 1$. This type of results have been pointed out for similar problems in [5].

A . Brouwer degree

There are many ways for defining Brouwer degree (see for example [22]). An intuitive one is the following : let us consider a continuous mapping F on the closed disk $\bar{D}(O,R)$ centered at the origin in $\mathbb{R}^2$:

$$F : \bar{D}(O,R) \to \mathbb{R}^2$$

As x travels along $\partial D(O,R)$ once around the origin in a positive sense, the image points $F(x)$ travel along an oriented curve C. We suppose that $O \notin C$. If n_+ and n_- denote the number of windings around the origin in a positive and negative sense then the degree is defined as

$$\deg(F, D, O) = n_+ - n_-$$

A consequence of this definition is that if $\deg(F,D,O) \neq 0$ then there exists $x_0 \in D(O,R)$ such that $F(x_0) = 0$.

An equivalent analytical definition of the degree can be stated as follows :

Assume that Ω is a bounded domain of $\mathbb{R}^n$, $F \in C^1(\Omega;\ \mathbb{R}^n)$ and $y \notin F(\partial\Omega) \cup F(S)$ where $S = \{x \in \Omega;\ F'(x) = 0\}$ (F' is the Jacobian matrix) then the Brouwer degree of the mapping F relatively to Ω and y is defined as

$$\deg(F, \Omega, y) = \sum_{x \in F^{-1}(y)} sign\, F'(x)$$

If $F : [a,b] \to \mathbb{R}$ with $F(a)$ and $F(b) \neq 0$ then an easy computation leads to

$$\deg(F,\ ]a,b]\,, 0) = \begin{cases} 0 & if\ F(a)\,F(b) > 0 \\ 1 & if\ F(a) < 0\ \ and\ F(b) > 0 \\ -1 & if\ F(a) > 0\ \ and\ F(b) < 0 \end{cases}$$

Thus $\deg(F,]a,b]\,, O) \neq 0$ always implies the existence of a solution of $F(x) = 0$ in $]\,a,b[$. This is nothing less than the classical intermediate-value theorem and the degree is a useful tool for generalizing this property.

Acknowledgement We thank Philippe Lecomte (INRA Sophia-Antipolis, France) for providing us biological images.

References

[1] R.A. Adams. *Sobolev Spaces.* Academic Press, New York, 1975.

[2] G. Alberti, S. Baldo, and G. Orlandi. Variational convergence for functionals of Ginzburg-Landau type, 2003. Preprint.

[3] L. Ambrosio and H.M. Soner. Level set approach to mean curvature flow in arbitrary dimension. *Journal of Differential Geometry*, 43, 1996.

[4] G. Aubert and L. Blanc-Feraud. Some remarks on the equivalence between 2d and 3d classical snakes and geodesic active contours. *IJCV*, 34(1):19–28, 1999.

[5] G. Aubert, L. Blanc-Féraud, and R. March. Γ-convergence of discrete functionals with non-convex perturbation for image classification, 2004. to appear in the SIAM Journal on Numerical Analysis.

[6] G. Aubert and P. Kornprobst. *Principle and applications of imaging radar*, volume 2 of *Manual of Remote Sensing*. J. Wiley and Sons, third edition, 1998.

[7] G. Aubert and P. Kornprobst. *Mathematical Problems in Image Processing*, volume 147 of *Applied Mathematical Sciences*. Springer-Verlag, 2002.

[8] F. Bethuel, H. Brezis, and F. Helein. *Ginzburg-Landau vortices*. Progress in Nonlinear Differential Equations and Their Applications. Birkhauser, 1994.

[9] V. Caselles, F. Catte, T. Coll, and F. Dibos. A geometric model for active contours. *Numerische Mathematik*, 66:1–31, 1993.

[10] V. Caselles, R. Kimmel, and G. Sapiro. Geodesic active contours. *IJCV*, 22(1):61–79, 1997.

[11] X.Y. Chen, S. Jimbo, and Y. Morita. Stabilization of vortices in the Ginzburg-Landau equation with variable diffusion coefficients. *SIAM Journal Math. Anal*, 1998.

[12] G. Gilboa, Y.Y. Zeevi, and N. Sochen. Complex diffusion processes for image filtering. In *Scale-Space '01*, volume 2106 of *Lecture Notes in Computer Science*, 2001.

[13] V. Ginzburg and L. Landau. On the theory of superconductivity. *Zheksper. Teo. Fiz*, 20, 1950.

[14] H. Grossauer. A combined PDE and textures synthesis approach to inpainting. In *ECCV 2004*, volume 3024 of *Lecture Notes in Computer Science*, May 2004.

[15] H. Grossauer and O. Scherzer. Using the complex Ginzburg-Landau equation for digital inpainting in 2D and 3D. In *Scale-Space '03*, volume 1682 of *Lecture Notes in Computer Science*, 2003.

[16] L. Lorigo, O. Faugeras, W. Grimson, R. Keriven, and C.F. Westin. Co-dimension-two geodesic active contours for the segmentation of tubular structures. In *Int. Conf. Information Processing in Medical Imaging*, 1999. Visegrad, Hungary.

[17] R. Malladi, J.A. Sethian, and B.C. Vemuri. Evolutionary fronts for topology-independent shape modeling and recovery. In *ECCV 1994*, volume 800 of *Lecture Notes in Computer Science*, pages 3–13, 1994.

[18] S. Osher and R.P. Fedkiw. Level set methods: An overview and some recent results. *Journal of Computational Physics*, 169:463–502, 2001.

[19] S. Ruuth, B. Merriman, J. Xin, and S. Osher. Diffusion-generated motion by mean curvatures for filaments, November 1998. Technical Report 98-47, UCLA Computational and Applied Mathematics.

[20] E. Sandier and S. Serfaty. A rigorous derivation of a free-boundary problem arising in superconductivity. *Annales Scientifiques de l'ENS*, 33(4), 2000.

[21] M. Sussman, P. Smereka, and S. Osher. A level set approach for computing solutions to incompressible two-phase flow. *Journal of Computational Physics*, 114:146–159, 1994.

[22] Zeidler. *Nonlinear Functional Analysis and its Applications, I, Fixed-Point Theorems*. Springer Verlag, 1986.